

Process mining-driven modeling and simulation to enhance fault diagnosis in cyber-physical systems

Francesco Vitale^a, Nicola Dall’Ora^{b,c}, Sebastiano Gaiardelli^b, Enrico Fraccaroli^b,
Nicola Mazzocca^a, Franco Fummi^b

^aUniversity of Naples Federico II, Department of Electrical Engineering and Information Technology,
Via Claudio, 21, Naples, 80125, Italy

^bUniversity of Verona, Department of Engineering for Innovation Medicine
(Section of Engineering and Physics), Strada le Grazie, 15, Verona, 37134, Italy

^cGuglielmo Marconi University, Department of Engineering Sciences, Via Plinio, 44, Rome, 00193, Italy

Abstract

Fault diagnosis in Cyber-Physical Systems (CPSs) is essential for ensuring system dependability and operational efficiency by accurately detecting anomalies and identifying their root causes. However, the manual modeling of faulty behaviors often demands extensive domain expertise and produces models that are complex, error-prone, and difficult to interpret. To address this challenge, we present a novel unsupervised fault diagnosis methodology that integrates collective anomaly detection in multivariate time series, process mining, and stochastic simulation. Initially, collective anomalies are detected from low-level sensor data using multivariate time-series analysis. These anomalies are then transformed into structured event logs, enabling the discovery of interpretable process models through process mining. By incorporating timing distributions into the extracted Petri nets, the approach supports stochastic simulation of faulty behaviors, thereby enhancing root cause analysis and behavioral understanding. The methodology is validated using the Robotic Arm Dataset (RoAD), a widely recognized benchmark in smart manufacturing. Experimental results demonstrate its effectiveness in modeling, simulating, and classifying faulty behaviors in CPSs. This enables the creation of comprehensive fault dictionaries that support predictive maintenance and the development of digital twins for industrial environments.

Keywords: Fault diagnosis, Simulation, Modeling, Classification, Process mining.

1. Introduction

The integration of *physical* and *cyber* processes in modern Cyber-Physical Systems (CPSs) offers significant opportunities to enhance service quality, reliability, and sustainability in critical sectors such as power grids, water management systems, precision agriculture, healthcare monitoring, and advanced manufacturing (Oks et al., 2024). Achieving high dependability requires robust fault diagnosis capabilities to detect anomalies, determine their root causes accurately, and proactively plan recovery actions (Ming et al., 2025). Additionally, simulation frameworks have become indispensable tools for accelerating CPS development, performing what-if analyses, and designing effective recovery strategies (Gueuziec et al., 2023; Tampouratzis et al., 2023).

Fault diagnosis in CPSs extends beyond simple anomaly detection to encompass a comprehensive understanding of fault propagation, root-cause analysis, and informed recovery decision-making (Cai et al., 2017; Yu & Zhao, 2020; Li et al., 2023). Modeling and simulation thus become essential for offering insights into complex system dynamics and enabling actionable recovery plans. Traditional fault modeling methods have employed various formalisms, such as Petri nets, Markov models, and domain-specific languages. Among these, Petri

nets have gained wide acceptance due to their clear, process-based semantics, facilitating interpretability, an increasingly critical attribute in trustworthy artificial intelligence applications (Hu et al., 2024; van der Aalst & Carmona, 2022; H. Liu et al., 2022; Mozafari Mehr et al., 2023).

Despite these advancements, a notable gap persists regarding unsupervised, data-driven modeling of faulty CPS behaviors directly from low-level sensor data, particularly within frameworks offering both predictive power and explanatory transparency. In fact, unsupervised approaches to anomaly detection aim to model normal patterns in historical time series and flag anomalous trends, which, however, do not provide further information about the type of anomaly that occurred (Belay et al., 2024). Besides, these approaches are often based on advanced deep learning methods, which, although powerful and extremely accurate, have explainability issues (Hanga et al., 2020). To bridge this gap, we propose a novel fault diagnosis methodology driven by process mining. Our approach combines collective anomaly detection in multivariate time series with process mining to extract interpretable Petri nets, thus effectively balancing accuracy and transparency, two critical dimensions in modern CPS fault diagnosis. The proposed methodology begins with isolating anomalous CPS behaviors, then converts sensor data into structured event logs, and finally

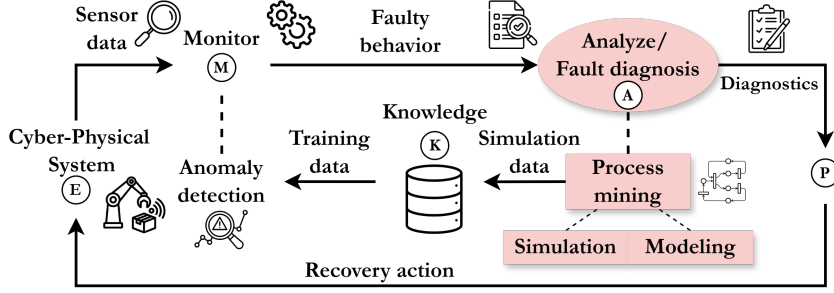


Figure 1: The MAPE-K loop for digital twin development in which the *analyze phase* (highlighted in red) implements the modeling and simulation parts of the proposed methodology.

extracts high-quality Petri nets. Enriched with precise timing distributions, these Petri nets enable detailed stochastic simulations, providing more insights into system behavior, generating more data for the knowledge base of the CPS, and supporting robust fault classification.

In summary, this paper contributes the following:

- A novel unsupervised fault diagnosis methodology driven by process mining to systematically isolate and interpretably model faulty CPS behaviors from raw sensor data.
- Extraction of interpretable, high-fidelity Petri nets enriched with timing distributions, enabling accurate fault replication through stochastic simulation.
- Empirical evaluation demonstrating the methodology’s capabilities in modeling accuracy, simulation fidelity, and fault classification effectiveness, validated on the Robotic Arm Dataset (RoAD), a recognized CPS manufacturing benchmark.

We contextualize our work within the Monitor-Analyze-Plan-Execute over a shared Knowledge (MAPE-K) loop (see Figure 1), a well-established framework for digital twin implementations (Feng et al., 2022). Our methodology specifically strengthens the *Analyze phase* through enhanced modeling and simulation capabilities, linking offline root-cause analysis with online anomaly classification. This integration significantly improves informed decision-making and facilitates proactive corrective actions.

The remainder of the article is structured as follows: Section 2 reviews relevant literature on process mining and Petri nets, positioning our contributions clearly within the existing state-of-the-art. Section 3 details the proposed unsupervised fault diagnosis methodology. Section 4 empirically assesses the methodology’s effectiveness using the RoAD benchmark. Finally, Section 5 summarizes key insights and outlines potential future research directions.

2. Background

Fault diagnosis in CPSs is intrinsically difficult. Hybrid continuous/discrete dynamics, large-scale multivariate sensor streams, and the stringent demand for interpretable decisions in

safety-critical domains jointly raise technical and methodological challenges. Classical solutions ranging from first-principles physical models and fuzzy rule bases to neural network driven classifiers have proven effective in specific settings; yet they typically (i) require extensive domain expertise, (ii) offer limited transparency, and (iii) provide little support for realistic behavioral simulation (Hanga et al., 2020).

To address these limitations, we propose a process mining-driven fault diagnosis methodology that effectively integrates data-driven learning with the formal structure of Petri nets, whose synergy with data-centric approaches has been demonstrated in prior works (da Silveira et al., 2025; Lassoued & Schwung, 2024; Nadim et al., 2022). Unlike black-box models, process mining generates explicit, executable representations of system behavior, thereby supporting both root-cause analysis and what-if exploration. Importantly, the proposed pipeline discovers such models *unsupervisedly* from raw sensor data, an essential capability when labeled fault instances are sparse. The remainder of this section introduces the necessary preliminaries on process mining and Petri nets, then surveys existing CPS fault-diagnosis research to position our contribution.

2.1. Preliminaries

Process mining comprises two core activities: *process discovery* and *conformance checking* (van der Aalst & Carmona, 2022). Process discovery builds a process model (here, a Petri net) from historical event logs, whereas conformance checking quantifies how closely new logs align with a reference Petri net. An event log is a collection of *cases*; each case records a time-ordered sequence of *events* corresponding to state transitions in the underlying CPS.

Definition 2.1 (Event, trace, case, event log). *Let \mathcal{E} be the universe of events, \mathcal{ST} the universe of state transitions, and \mathcal{T} the universe of timestamps. For $e \in \mathcal{E}$, denote its state transition and timestamp by $\#_{st}(e) \in \mathcal{ST}$ and $\#_t(e) \in \mathcal{T}$, respectively. A trace is an ordered sequence $\sigma = \langle e_1, \dots, e_k \rangle$ with $e_i \in \mathcal{E}$; the set of all traces is \mathcal{E}^* . Let \mathcal{C} denote the universe of cases and $\#_{trace}(c) \in \mathcal{E}^*$ the trace associated with case $c \in \mathcal{C}$. An event log is a finite subset $L \subseteq \mathcal{C}$.*

In this study, we focus on the control-flow relations and timing distributions extracted from event logs and captured via labeled Petri nets.

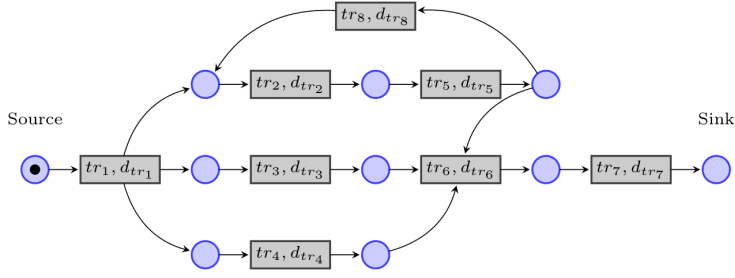


Figure 2: Illustrative workflow stochastic Petri net with transitions tr_1, \dots, tr_7 and associated firing-time distributions $d_{tr_1}, \dots, d_{tr_7}$.

Definition 2.2 (Labeled Petri net). *Let P and Tr be disjoint node sets ($P \cap Tr = \emptyset$) in a bipartite graph, and let $F \subseteq (P \times Tr) \cup (Tr \times P)$ be the set of directed arcs. A Petri net is the triple (P, Tr, F) . Its marking $M \in \mathcal{B}(P)$ is a multiset of tokens and encodes the current state. Furthermore, consider a set of state transitions $ST \subseteq \mathcal{ST}$ and a labeling function $l_{Tr} : Tr \rightarrow ST \cup \{\tau\}$, where τ denotes a silent (unobservable) transition. A labeled Petri net is the tuple (P, Tr, F, ST, l_{Tr}) . \mathcal{N} denotes the universe of all labeled Petri nets, hereafter referred to as Petri nets.*

The formal semantics of Petri nets include the ability to *fire* a transition. Given the number of incoming arcs of a transition, if there is at least a token in each place connected to the transition, it can fire, i.e., the transition consumes one token from each incoming place and generates one token for each outgoing arc. This firing dynamic allows the Petri net to evolve its state, and enables the above-mentioned conformance checking and simulation. In addition, it is worth noting that there is a special class of Petri nets, namely workflow Petri nets, which have two specific places: a source place and a sink place. The initial marking only assigns a token to the source place. Any complete firing sequence moves the initial marking to the final marking, which consists of at least a token in the sink place.

A desirable property of Petri nets is the *soundness*. A Petri net is sound if any firing sequence from the initial marking can reach a unique final marking without leaving dead transitions (van der Aalst & Carmona, 2022). If each transition is further annotated with a random firing time, also known as its firing rate, the model becomes a *stochastic Petri net* (Wittbold et al., 2023).

Definition 2.3 (Stochastic Petri net). *Given a Petri net $N = (P, Tr, F, ST, l_{Tr}) \in \mathcal{N}$, let \mathcal{D} be a set of probability distributions and $\delta : Tr \rightarrow \mathcal{D}$ assign each transition $tr \in Tr$ its firing-time distribution d_{tr} . The triple $N_S = (N, \delta, \mathcal{D})$ is termed a stochastic Petri net.*

In the following, we will aim to build stochastic workflow Petri nets. Figure 2 exemplifies such a model. By repeatedly sampling firing times and resolving race conditions (Rogge-Solti et al., 2014), one can replay this model to simulate realistic CPS traces.

2.2. Related Works

To further contextualize our contribution, we revisit traditional model-based techniques, followed by hybrid approaches that attempt to incorporate data-driven insights into Petri net-based fault diagnosis.

2.2.1. Model-based approaches

Early research on fault diagnosis in industrial systems proposed Petri nets as a reasoning tool to understand the root causes of system-wide failures (Mansour et al., 2013). Subsequently, research sought to synchronize the fault-free and faulty behaviors within the same Petri net, which enabled modeling controllers to identify faults and enforce recovery actions to ensure system safety. For example, S. Liu et al. (2013) modeled the fault-error-failure chain of a home CPS using a stochastic Petri net, pairing model elements with the layered view of the system. Furthermore, Nazemzadeh et al. (2013) proposed a method to integrate faults in fault-free Petri nets. They defined fault models as tuples of Petri net elements, including faulty transitions whose activation leads to errors.

The diagnosability of faults on Petri nets depends on whether the observed behavior provides sufficient information to identify the activation of faulty transitions. To check if observed behavior causes the activation of faulty transitions, a diagnoser, which is a model-checking routine, determines the activation of faulty transitions. Several proposals have introduced different diagnosers based on the assumptions about the reference Petri net (e.g., transition types and labeling) and the model-checking routine used (e.g., integer linear programming) (Cabasino et al., 2011; Bonafin et al., 2022; J. Liu et al., 2024).

2.2.2. Hybrid approaches

Modeling Petri nets for complex CPSs is challenging and error-prone (Bourdeau et al., 2019). Consequently, researchers have begun to leverage data-driven insights to integrate faulty behavior into fault-free Petri nets. For example, Zhu et al. (2019) formulated a set of integer linear programming constraints to incorporate faulty behavior into fault-free Petri nets and identify the root causes of faults. Similarly, Hou et al. (2021) proposed an alternative data-driven method to discover faulty Petri nets. This method utilizes transition incidence matrices obtained from system traces to address the NP-hard nature of integer linear programming approaches.

Table 1: Representative hybrid Petri-net approaches: input data granularity, methodological focus, diagnostic strategy, and availability of simulation support.

Reference	Data type	Approach	Fault diagnosis	Sim.
(Zhu et al., 2019)	High-level event data	Integer linear programming	Data-driven extension of a fault-free Petri net to include faulty transitions	No
(Hou et al., 2021)	High-level event data	Transition incidence matrices	Data-driven extension of a fault-free Petri net to include faulty transitions	No
(Neshastegaran et al., 2022)	High-level event data	Process discovery	Data-driven modeling of the overall behavior of an industrial system with the Petri net to reason about the root causes of faulty behavior	No
(Friederich & Lazarova-Molnar, 2022)	High-level event data	Process discovery	Data-driven modeling of the normal behavior of an industrial system with the Petri net and ad-hoc introduction of faulty behavior into the model	No
(Wang et al., 2022)	High-level event data	Process discovery and conformance checking	Data-driven modeling of the normal behavior of information systems with the Petri net and verification of deviations from the model of run-time data	No
(Vitale et al., 2023)	Low-level sensor data	Process discovery and conformance checking	Data-driven modeling of the normal behavior of an industrial system with the Petri net and verification of deviations from the model of run-time data	No
(Shi et al., 2024)	Low-level sensor data	Process discovery	Data-driven modeling of the normal behavior of an industrial system with the Petri net and verification of deviations from the model of run-time data	No
(De Benedictis et al., 2023)	High-level event data	Conformance checking	Verification of deviations from the Petri net of run-time data	Yes
(Beyel et al., 2024)	High-level event data	Process discovery	Data-driven modeling of the overall behavior of an industrial system with the Petri net to reason about the root causes of faulty behavior	No
(Vitale et al., 2025)	Low-level sensor data	Process discovery and conformance checking	Data-driven modeling of the normal behavior of an industrial system with the Petri net and verification of deviations from the model of run-time data	Yes
Our work	Low-level sensor data	Process discovery and conformance checking	Data-driven modeling of the faulty behavior of an industrial system with the Petri net to reason about the root causes of faulty behavior	Yes

More recently, process mining has been applied to fault diagnosis and simulation. Neshastegaran et al. (2022) developed the topology of an industrial plant via process discovery, leveraging monitored events to improve the understanding of potential faults. Friederich and Lazarova-Molnar (2022) proposed a process mining-based framework for reliability modeling of smart manufacturing processes. The framework integrates the fault-free Petri net obtained through process discovery with custom fault models for each manufacturing resource. Wang et al. (2022) set forth a method combining neural network-based anomaly detection with process mining. Their method first involves modeling normal behavior with a Petri net from discrete logs collected from, e.g., network data and software executions. Next, they perform neural network-based anomaly detection to identify anomalous traces in run-time event logs. Finally, the anomalous traces are checked against the normal behavior to analyze the deviations and provide an explanation of the deviating behavior. Vitale et al. (2023) and Shi et al. (2024) proposed using process discovery and conformance checking to characterize normal behavior from low-level sensor data of industrial systems through Petri nets and check deviations from such behavior. They proposed different unsupervised techniques to discretize sensor data and enable using process discovery and conformance checking. De Benedictis et al. (2023) used conformance checking to evaluate whether digital twins could detect new runtime faults. These faults arise from faulty simulations generated from a Petri net of a proof-of-concept Industrial Internet of Things application. Beyel et al. (2024) introduced a method of connecting high-level event data from a CPS in the automotive domain with Petri nets developed through process discovery. They demonstrated how this method enables the analysis of time spent in CPS states and the frequency of the transitions between them over time. Vitale et al. (2025) provided an unsupervised approach to characterizing the state transitions of an industrial CPS involving a real water distribution testbed case study. Their approach involved characterizing the normal CPS behavior through process discovery and checking any deviations from it through conformance checking.

Distinctive contribution. Unlike prior work, our method (i) operates directly on *low-level sensor data*, (ii) *unsupervisedly* mines interpretable workflow labeled Petri nets that isolate specific faulty behaviors, and (iii) enriches these nets with timing information to enable stochastic replay for root-cause analysis and fault dictionary construction. Table 1 summarizes the principal contributions and delineates the niche addressed by the present study.

3. Methodology

This section explores the steps of the proposed unsupervised process mining-driven fault diagnosis methodology, as illustrated in Figure 3. The methodology is organized into four sequential services implemented by three components within a digital twin. These components are: an anomaly detector implementing time-series *anomaly detection* to identify anomalous time series windows; a modeler implementing *event log*

extraction to convert CPS dynamics into event logs and *process mining* to extract a stochastic Petri net and evaluate its quality; a simulator implementing *simulation* to generate variants of the modeled faulty scenarios. Each component depends on the knowledge database, which collects historical data from both past data collection campaigns and simulations, stores a set of stochastic Petri nets isolating the different faulty CPS behaviors, and maintains a set of control rules to plan recovery actions in response to specific faults that occur in the physical plant. In the following, we provide a detailed description of each service offered by the methodology.

3.1. Anomaly detection

Anomaly detection in multivariate time series has become highly effective, especially due to advancements in deep learning approaches that can accurately discriminate normal patterns from anomalous ones (Zamanzadeh Darban et al., 2024; Chatterjee & Ahmed, 2022; Cook et al., 2020). Typically, these approaches aim to model normal patterns in historical time series and flag anomalous trends. Due to the scarcity of anomalous samples, most multivariate time series anomaly detection approaches concentrate on modeling the normal behavior of the target system (Belay et al., 2024). While these approaches have achieved excellent results, they are unable to classify the specific anomaly that occurred. In light of this, our proposal involves first isolating anomalous trends in time series and then modeling these trends through process mining. Hence, this first step leverages multivariate time series anomaly detection to distinguish normal behavior from anomalies. Specifically, we aim to detect collective anomalies, defined as sequences of contiguous samples that deviate from expected patterns (Chandola et al., 2012; Qin et al., 2023). We refer to such sequences as **anomalous time series windows**.

Definition 3.1 (Time series window). *Let us denote \mathcal{T}_o the set of timesteps up to $o \in \mathbb{N}$. Let $ts \in \mathbb{R}^{o \times p}$ be a multivariate time series with p features and o values. Let $ts(i) \in \mathbb{R}^p$ be time series values at timestep $t_i \in \mathcal{T}_o$. Let $t_k, t_l \in \mathcal{T}_o, k < l \leq o$. A time series window $ts_{k,l}$ is the set*

$$ts_{k,l} = \{ts(t_j) \in \mathbb{R}^p : t_j \in \mathcal{T}_o, t_k \leq t_j \leq t_l\}. \quad (1)$$

Once the anomalous time series windows are isolated from the multivariate time series, they are passed on to the next step for event log extraction.

3.2. Event log extraction

Creating an anomalous event log from anomalous time series windows involves characterizing data as sequences of events. Common approaches for discretizing time series data and extracting event logs involve grouping each sample into clusters (Hemmer et al., 2021; Vitale et al., 2023; Su et al., 2025) or by identifying specific events, such as increasing or decreasing trends and specific activities (van Eck et al., 2016; Shi et al., 2024; Vitale et al., 2025). While the latter approaches are more precise in identifying events from sensors data, they require domain knowledge and, in some cases, accurate labeling. On the

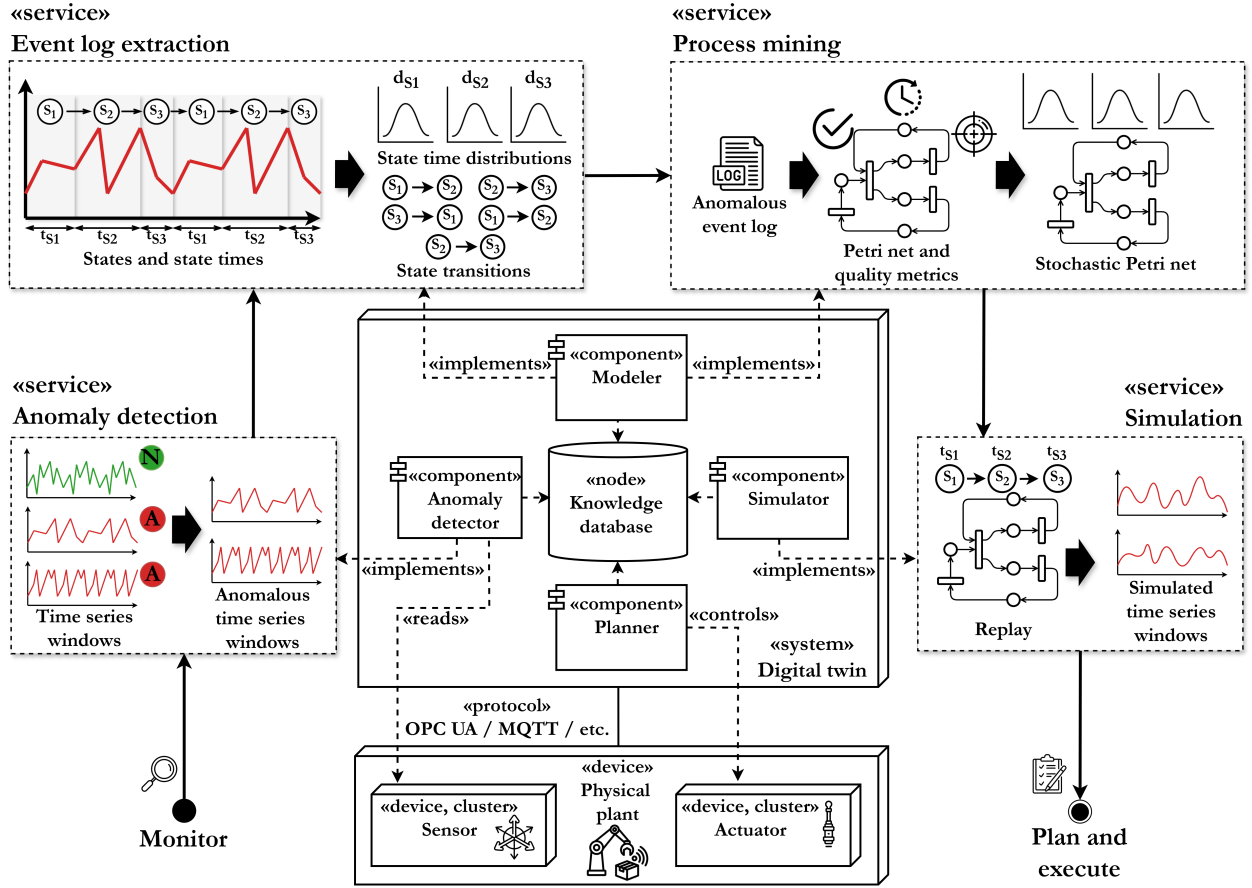


Figure 3: The unsupervised process mining-driven methodology to enhance fault diagnosis in cyber-physical systems, organized as four services implemented by the digital twin of a physical plant: anomaly detection to identify anomalous time series windows, event log extraction to obtain anomalous event logs and the corresponding state and state times, process mining to capture faulty behavior through a stochastic Petri net, and simulation to generate new time series reflecting the faulty CPS behavior.

other hand, clustering-based approaches are unsupervised and very valuable in contexts where the collected data is not labeled or the manual identification of possible trends is impractical. Hence, our proposal adopts the first class of methods and clusters time series values into a set of **states** and collects events by identifying transitions between clusters, i.e., the **state transitions**.

Definition 3.2 (State and state transition). Let $ts \in \mathbb{R}^{o \times p}$ be a multivariate time series with p features and o values and $\mathcal{S} = \{s_1, \dots, s_\alpha : s_i \in \mathbb{R}^p, \alpha \in \mathbb{N}\}$ be a set of α clusters. $s_t \in \mathcal{S}, t \in \mathcal{T}_o$ is the state associated with $ts(t)$, hence \mathcal{S} is the set of states. Given $t_k, t_l : 0 \leq k < l \leq o$, there is a state transition associated with t_l if $\forall t_j : t_k < t_j < t_l, s_{t_j} = s_{t_k}$ and $s_{t_k} \neq s_{t_l}$. An event e associated with the pair of states s_{t_k}, s_{t_l} is such that $\#_{st}(e) = st_l = s_{t_k} \rightarrow s_{t_l}$ and $\#_t(e) = t_l$. The state s_{t_k} is associated with st_l .

The state transitions from the anomalous time series windows are collected to build an **anomalous event log**. The timestamps associated with the state transitions are also recorded. Each anomalous time series window corresponds to a single case in the anomalous event log. Each case contains the state transitions and corresponding timestamps associated with the respective anomalous time series window. Finally, the **state**

times and state time distributions are collected by considering the state transitions associated with the events of the anomalous event log.

Definition 3.3 (State time and state time distribution). Let \mathcal{S} be a set of states, $e \in \mathcal{E}$ be an event, and $\#_{st}(e) = s_{t_k} \rightarrow s_{t_l}$ a state transition. The state time of $s_{t_k} \in \mathcal{S}$ associated with $\#_{st}(e)$ is $t_l - t_k$. The state time distribution of state $s_{t_k} \in \mathcal{S}$ is a function $d_s : \mathbb{R} \rightarrow \mathbb{R}$ obtained by collecting all the state times of s_{t_k} .

The state time distributions compose **event log statistics** used in the subsequent step to integrate the time perspective into process mining.

3.3. Process mining

Using the anomalous event log, a process discovery algorithm identifies the control-flow relations between state transitions from the individual cases within the anomalous event log. These control-flow relations are encoded into a **Petri net**, which represents the system's behavior under faulty conditions.

Definition 3.4 (Process discovery algorithm). Let $L \subseteq C$ be an anomalous event log. A process discovery algorithm is a function γ that captures the control-flow relations among the

state transitions of the cases of L and converts them to a Petri net $N \in \mathcal{N}$: $\gamma(L) = N$.

The set of control-flow relations discovered by γ depends on the specific process discovery algorithm being used. For example, the inductive miner (Leemans et al., 2013) identifies several types of control-flow relations, such as sequence, parallel, exclusive, and redo-loop relations. It does this by splitting the event log into simpler segments, which enables the recognition of these relations. The integer linear programming-based miner (van Zelst et al., 2018) finds causal relations between the activities of an event log and specifies a system of inequalities to find the so-called regions, i.e., two sets of activities such that the prior execution of the first set enables the execution of the second set. Notably, both the inductive miner and integer linear programming-based miner discover workflow Petri nets. The types of control-flow relations identified by the process discovery algorithm determine the range of possible Petri nets the algorithm can generate. This limitation is known as the *representational bias* and significantly impacts the quality of the resulting Petri net (van der Aalst & Carmona, 2022). For example, although the inductive miner builds perfectly fitting Petri nets from the data, it forces this property by introducing many silent transitions. This makes the resulting Petri net “underfitting”, i.e., it introduces many more behaviors than the ones present in the observed data. Yet, while the integer linear programming-based miner limits the introduction of silent transitions, it enforces many constraints in building the above-mentioned regions through the system of inequalities, hence leading to “overfitting” Petri nets, i.e., the model is very specific for the data at hand. To mitigate the underfitting and overfitting phenomena, both algorithms were extended with filtering mechanisms that allow reducing the impact of these two effects on the resulting Petri net (van der Aalst & Carmona, 2022).

To evaluate the **quality metrics** of the resulting Petri nets, conformance checking can be used. The state-of-the-art approach to conformance checking is the alignment-based variant (Carmona et al., 2018), which compares how closely the event log matches the behavior modeled by the Petri net. For instance, if a trace from the event log violates the rules of the Petri net – such as having incorrectly ordered or skipped state transitions – alignment-based conformance checking identifies the discrepancy. It then constructs a model trace that correctly pairs with the log trace. The model trace represents a valid sequence according to the Petri net, but it might not match the sequence recorded in the event log. The model trace is also adjusted to minimize a cost function, reflecting the event log deviation. The alignment that results in the lowest cost is called the *optimal alignment*, whereas the one with the highest cost is called the *worst alignment*. Alignments can be used to evaluate fitness and precision. On the one hand, fitness measures how closely the event log aligns with the Petri net by comparing the model traces with the corresponding real traces. On the other hand, precision measures how tailored the Petri net is to the event log by evaluating how much behavior is enabled when the traces are replayed on the Petri net to calculate the alignments (Adriansyah et al., 2015). Both fitness and preci-

sion should be balanced to ensure that the Petri net is neither underfitting nor overfitting.

Once a quality Petri net is built with process discovery, process enhancement is performed to associate time information with the Petri net (van der Aalst & Carmona, 2022). In this case, state transitions are associated with the state time distributions obtained in the event log extraction phase. Hence, process enhancement leads to a **stochastic Petri net** that resembles the faulty CPS behavior. This Petri net is used in the subsequent simulation phase to further analyze the fault. In addition, this Petri net can also be used for fault classification. Both these use cases are empirically evaluated in Section 4.

3.4. Simulation

The simulation **replays** a stochastic Petri net to generate new traces. A simulated trace is of the form $\langle st_1, \dots, st_f \rangle$. A state is associated with each state transition of the trace. E.g, if $st_1 = s_\beta \rightarrow s_\gamma$, with s_β and s_γ being two states of the CPS, then s_β is associated with st_1 . At each state in the simulated trace, a corresponding state time is randomly selected from the state time distribution linked with that transition. As a result, the sequence of state transitions is transformed into state-state time pairs. The sequence of state-state time pairs is the **simulated time series window**.

Definition 3.5 (Simulated time series window). *Let $N \in \mathcal{N}$ be a Petri net, $\mathcal{S} = \{s_1, \dots, s_\alpha : s_i \in \mathbb{R}^p, \alpha \in \mathbb{N}\}$ a set of α states, $\mathcal{D} = \{d_1, \dots, d_\alpha : d_i : \mathbb{R} \rightarrow \mathbb{R}, \alpha \in \mathbb{N}\}$ the set of state time distributions, δ the function that associates the state time distributions with the state transitions of N , and $N_S = (N, \delta, \mathcal{D})$ a stochastic Petri net. Let $\sigma_{sim} = \langle st_1, \dots, st_k \rangle$ be a trace of k state transitions obtained by replaying N_S . The corresponding simulated time series window is the sequence of pairs $\langle (s_{st_1}, t_{st_1}), \dots, (s_{st_k}, t_{st_k}) \rangle$. The i -th pair (s_{st_i}, t_{st_i}) captures the state $s_{st_i} \in \mathcal{S}$ associated with st_i and the corresponding state time t_{st_i} sampled from \mathcal{D} .*

The simulated time series windows closely mimic the behavior of the CPS under faulty conditions. As a result, these time series can be utilized, for example, for data augmentation, enhancing both anomaly detection and fault diagnosis.

4. Evaluation

The goals of the experiments involve analyzing:

- The impact of key methodology factors on the unsupervised modeling and simulation quality of faulty CPS behaviors (modeling and simulation quality).
- The ability to identify different faulty CPS behaviors and clearly distinguish them from one another to build a fault dictionary (fault identification).

For these purposes, we apply the methodology to the Robotic Arm Dataset (ROAD) case study (Mascolini et al., 2023), whose dataset is one of the best representatives in the manufacturing CPS context, as reported in the work of Golendukhina et

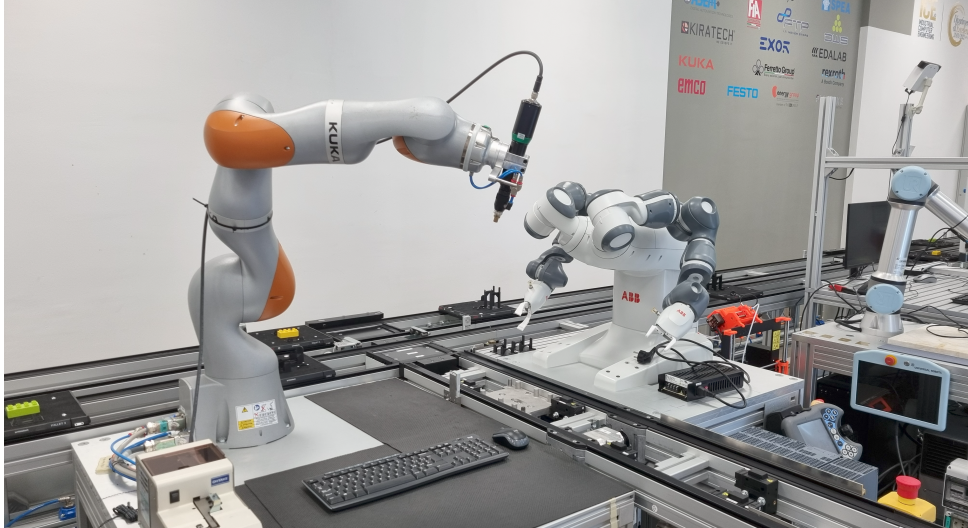


Figure 4: Experimental setup of the Robotic Arm Dataset (RoAD) testbed at the University of Verona. The smart manufacturing line integrates collaborative robots from KUKA, ABB, and Universal Robots, enabling realistic simulation and acquisition of low-level sensor data for fault diagnosis and digital twin development.

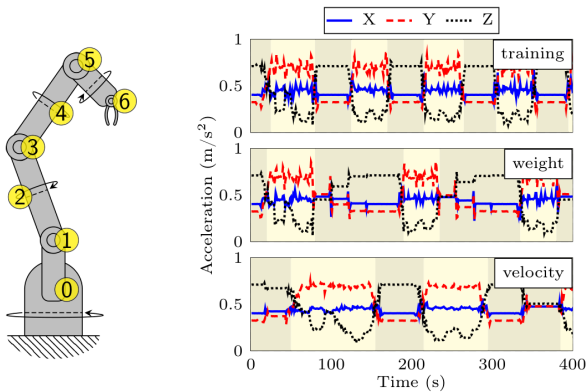


Figure 5: Case study presented in the ROAD dataset with labels showing the positions of the sensors on the robotic arm (left), and graphs that depict the acceleration values measured by sensor 2 under diverse conditions, i.e., training/nominal behavior, and weight and velocity anomalies (right).

al. (2024) and Khan et al. (2025). We evaluate the methodology’s effectiveness in modeling and simulating faulty time series windows collected from the ROAD dataset. The discussion below describes the ROAD case study and the methodology application to it, an overview of the experiments, and a detailed discussion of the results, outlining the findings and potential threats to the validity of the experimentation.

4.1. The RoAD case study

Mascolini et al. (2023) presented the ROAD case study, specifically designed to support developing and testing machine learning-driven algorithms.

Physical plant. The ROAD case study comprises real multivariate time series data collected from various sensors mounted on a Kuka LBR iiwa robotic arm, a collaborative robotic arm deployed in a scale replica of a manufacturing process (see

Figure 4). Figure 5 (left) shows a schematic of the physical plant and the set of sensors, labeled 0 to 6, deployed across its structure. The robotic arm is integrated into a fully-fledged production line located in the Industrial Computer Engineering (ICE) Laboratory¹, a cutting-edge research facility at the University of Verona dedicated to cyber-physical production systems. This production line includes a diverse set of industrial-grade machines, representative of modern smart manufacturing environments: a *quality control cell* with high-resolution laser scanners and cameras for visual inspection, a *robotic assembly cell* with two collaborative robotic manipulators for flexible handling tasks, a *subtractive manufacturing cell* equipped with a four-axis computer numerical control milling machine, and a *functional control cell* that integrates a flying probe system for automated functional testing. Two automated guided vehicles manage the internal logistics, transporting goods between the *warehouse* and the *conveyor belt*, enabling the emulation of complex material flows. The Kuka robotic arm plays a pivotal role within this system, performing critical operations such as assembly, disassembly, and tightening. The production line is based on the flexible manufacturing paradigm. Rather than adhering to rigid, predefined workflows, it enables the dynamic composition of manufacturing processes by orchestrating a set of reusable processing capabilities offered by each work cell. This configuration not only mirrors the adaptability required in Industry 4.0 scenarios but also provides a high-fidelity experimental environment for evaluating advanced automation, orchestration strategies, and verification techniques under realistic conditions.

Sensor data. The multivariate time series include measurements from accelerometers, gyroscopes, and power consumption sensors. Additionally, the dataset features an “Anomaly” label indicating anomalies’ presence or absence. The recorded

¹<https://www.icelab.di.univr.it/laboratory>

multivariate time series reflect both nominal and anomalous behaviors of the Kuka LBR iiwa robotic arm. The identified anomalies are categorized into three distinct classes: collision, weight, and velocity anomalies. Furthermore, ROAD includes a metadata description that classifies each action performed by the robotic manipulator with a numeric value ranging from 0 to 30. Figure 5 (right) presents three sample time series from the ROAD dataset, depicting acceleration measurements on the X, Y, and Z axes recorded by sensor 2 under various conditions, including nominal (training) and faulty scenarios (weight and velocity anomalies). The left side of the figure illustrates a schematic of the Kuka LBR iiwa robotic manipulator, indicating the precise locations of each sensor. The training time series is composed of two normal patterns, highlighted in Figure 5 that repeat approximately every 100 seconds. The weight and velocity time series impact these patterns differently. Weight time series are characterized by an increase in the duration of the second pattern, while in the velocity time series, the duration of the first pattern is increased.

Methodology application. We aim to capture the faulty CPS behavior through our methodology as follows. First, we set out a controlled environment for the experiments by manually tuning the anomaly detection step to a fixed configuration, as evaluating the impact of the quality of anomaly detection on subsequent steps is out of scope. Next, we apply the event log extraction and process mining steps to either of the weight and velocity time series windows to obtain quality stochastic Petri nets capturing the faulty CPS behavior. Furthermore, we simulate for a given number of times the reference Petri net and evaluate the alignment of the simulated time series windows with the original faulty CPS behavior. Finally, we evaluate how effective our proposal is in regard to identifying different types of faults.

4.2. Experimental setup

Hardware and software specifics. The software for the experiments is implemented using Python and was run on a Windows 10 machine with an Intel® Core™ i9-11900K CPU @ 3.50GHz and 32GB of RAM. The software uses machine learning and PM libraries, such as `scikit-learn` and `pm4py`. In addition, it includes a set of DOS batch scripts to automatically replicate the experiments carried out in this work, publicly available on GitHub².

Data pre-processing, anomaly detection and simulation. The detailed analysis of data pre-processing and anomaly detection impact on the results is out of the scope of this work. Nonetheless, to set out a controlled environment for the experiments, we manually tuned these two steps according to the data at hand shown in Figure 5. First, training, velocity, and weight time series were normalized between -1 and 1. Second, 10000 samples for each time series of sensor 2 of the robotic arm were

retrieved. This selection is due to velocity and weight anomalies being particularly evident in the acceleration values captured by this sensor. Fourth, we set the window length to 100 seconds when extracting time series windows. This is because the training time series has a recurrent pattern of approximately 100 seconds. However, this split does not result in anomalous time series windows only. For example, by splitting the weight time series into time series windows of 100 seconds, we might include normal parts found in the training behavior, too. To isolate time series outlining anomalous behavior only, we use the algorithm proposed by Paparrizos and Gravano (2016), which correlates similar time series windows and divides them into different sets. We configured this procedure so that we could select the set that contained those anomalous time series windows highlighted in Figure 5. Finally, during the simulation we set the number of traces to simulate to 300 and, for each trace, generate the simulated time series according to Definition 3.5. This number of simulated time series windows was sufficient to extract a statistically reliable estimation of how different the simulated Petri net was compared to the actual time series windows.

Factors. The key methodology factors regarding the event log extraction and process mining steps of the methodology involve the clustering and process discovery algorithms. The clustering algorithm employed in the experiments to extract the state, state transitions, and state time from time series is K-means, which is a well-known clustering technique that links each data point to a single cluster. This technique is desirable as it allows the user to specify the desired number of clusters to be extracted. The K factor relates to how many states and state transitions can be captured. For example, if K equals 3, the CPS dynamics are discretized into 3 states and 6 state transitions. Hence, the higher K, the finer-grained the discretization is. The process discovery techniques used to extract the Petri net from the anomalous event log are the Inductive Miner Infrequent (IMf) (Leemans, Fahland, & van der Aalst, 2014) and Integer Linear Programming-based Miner (ILP) (van Zelst et al., 2018). These two techniques can tolerate noise in event logs and utilize two distinct approaches to discover control-flow relations, which allows evaluating the representational bias impact outlined in Section 3. To reduce the impact of noise in event logs as much as possible without too much filtering, we set the noise threshold of these two algorithms to 75%.

Metrics. The metrics used to evaluate the Petri net quality are fitness and precision, the metric to evaluate the similarity to the actual anomalous time series is the Root Mean Square Error (RMSE), the metric to evaluate the time complexity is the conformance checking time, namely the time required to check anomalous event logs on the reference Petri net, and the metrics to evaluate the space complexity of the Petri net are its number of places and number of arcs.

4.3. Modeling and simulation quality results

To assess the impact of the clustering and process discovery configurations on the fitness, precision, RMSE, conformance

²https://github.com/francescovitale/pm_based_modeling_simulation.

checking time, number of places and number of arcs metrics, we lay out a two-factor full factorial experiment, where the first factor is K, whereas the second factor is the process discovery algorithm. For each pair of factor values, the process mining-driven methodology is run 10 times to account for the randomness of time series windows sampling and the simulation. Tables 2 and 3 report the methodology results of the ILP and IMf regarding both the velocity and weight anomalies for each K value. Additionally, Figures 6 and 7 provide the error plots of both quality (fitness, precision, and RMSE) and complexity (conformance checking time, places, and arcs).

Quality metrics. The quality of the Petri net in terms of fitness and precision tends to drop for both the ILP and IMf as K increases. However, while this trend is valid for low K values, high K leads to uncertain results, as the standard deviation of both the fitness and precision increase as K increases. For example, considering the velocity anomaly, the ILP achieves 0.790 ± 0.284 fitness and 0.623 ± 0.225 precision for K equal to 12, outlining the unreliability of these two metrics as K increases. This is clear from the fitness and precision error bars in Figures 6 and 7. In general, however, the ILP achieves for both anomaly types overall better fitness and precision than the IMf, whose figures are consistently lower. The results also indicate that as K increases, the RMSE gradually decreases until it reaches its minimum point, after which it begins to rise. Specifically, the lowest values for the velocity anomaly are $0.064 m/s^2$ for the ILP with K equal to 9 and $0.067 m/s^2$ for the IMf with K equal to 9. Similarly, the lowest values for the weight anomaly are $0.050 m/s^2$ for the ILP with K equal to 8 and $0.061 m/s^2$ for the IMf with K equal to 10. Additionally, it is worth noting that very low K values lead to higher RMSE standard deviation. For example, considering the velocity anomaly, for K equal to 2 and 3, the ILP achieves, respectively, $0.079 \pm 0.034 m/s^2$ and $0.095 \pm 0.040 m/s^2$.

Complexity metrics. Conformance checking time increases for higher K values for both the ILP and IMf. However, as Figures 6 and 7 show, whereas such an increase is gradual for the ILP, it is very abrupt for the IMf. In fact, considering the velocity anomaly, the ILP only peaks at 1.896 ± 2.837 s for K equal to 12, whereas the IMf reaches 30.198 ± 32.030 s. In addition, the higher the K values, the higher the standard deviation of the conformance checking time for both the ILP and IMf. Regarding the space complexity, both algorithms lead to an abrupt increase in terms of the number of places and arcs. For example the ILP builds Petri nets of the velocity anomaly with up to 38 ± 11 places and 1132 ± 1419 arcs with K equal to 12, whereas the IMf builds Petri nets of the velocity anomaly with up to 33 ± 17 places and 1164 ± 627 arcs with K equal to 10. This leads to convoluted Petri nets that become harder to read and interpret.

Visualization. Figure 8 shows the simulated time series windows obtained by simulating the best stochastic Petri nets achieved through the ILP and IMf for both the velocity and weight anomalies, namely those achieved with K equal to 9 and

8 for the ILP and with K equal to 9 and 10 for the IMf. However, although these Petri nets result in low RMSE, they are quite complex with respect to both the number of places and the number of arcs. For visualization purposes, we instead show in Figure 9 the velocity and anomaly Petri nets obtained by the ILP with K equal to 4. Both the Petri nets have transitions associated with the state transitions unsupervisedly captured through clustering in the event log extraction process. Specifically, considering the velocity Petri net (left), the clustering process extracted four states, labeled 0, 1, 2 and 3, and by recording the state transitions within the time series windows, the resulting Petri net captures $0 \rightarrow 2, 0 \rightarrow 3, 1 \rightarrow 2, 2 \rightarrow 0, 2 \rightarrow 1, 3 \rightarrow 0$. While the velocity Petri net is quite simple to read, the weight Petri net is more complex, which could be due to noisier time series windows leading to more behavior being captured by a single Petri net.

4.4. Fault identification results

To evaluate whether the proposed methodology is able to not only simulate but also correctly distinguish faults from one another, we lay out a two-factor full factorial experiment. The first factor is K, whereas the second factor is the anomaly type, namely the velocity or weight anomaly. For each pair of factor values, the process mining-driven methodology is run 10 times to account for the randomness of time series windows sampling. We limit the analysis to the ILP, as it has shown the best modeling performance compared to the IMf with respect to quality and complexity.

Table 4 reports the results in terms of fitness values. In particular, $F_{Velocity}$ and F_{Weight} indicate, respectively, the fitness value against the velocity and weight Petri nets. Additionally, the ratio between the two indicates how effective the methodology allows discriminating the two faults. Figure 10 shows that high K values lead to better ratios, hence better fault identification. For example, with K equal to 12, the velocity Petri net fits the velocity anomaly ($F_{Velocity} = 0.793 \pm 0.234$) and does not fit the weight anomaly ($F_{Weight} = 0.220 \pm 0.070$), i.e., the velocity Petri net fits the actual anomaly 4.238 ± 2.422 better than the weight anomaly. However, it is worth noting that although high K values allow discriminating anomalies better, high K values also increase time and space complexity significantly, as Table 2 and Figure 6 highlight. Hence, one may settle for a slightly more underfitting yet interpretable velocity Petri net, such as the one shown in Figure 9 (left), which still discriminates the velocity anomaly from the weight anomaly with reasonable margin ($F_{Velocity}/F_{Weight} = 1.500 \pm 0.553$).

4.5. Discussion

Modeling and simulation quality. In this part of the experimentation, we evaluated whether the methodology allowed the extraction of fitting, precise, accurate, time-efficient, and readable Petri nets. The experiments outlined that increasing the K factor led to slightly lower Petri net quality in terms of fitness and precision yet more accurate simulations in terms of RMSE. However, this increase stops when the state space becomes too complex and makes the RMSE rise. This trend is true for both

Table 2: Methodology results of the ILP regarding the *velocity* and *weight* anomalies showing the mean fitness, precision, RMSE, conformance checking (CC) time, number of places, number of transitions, number of arcs, and size for each K. The grey rows outline the metrics related to the Petri nets in Figure 9. Highlighted in bold are the Petri nets with the lowest RMSE.

ILP (75% noise threshold)							
	K	F	P	RMSE ($\frac{m}{s^2}$)	CC time (s)	Places	Arcs
Velocity anomaly	2	0.898 ± 0.088	0.851 ± 0.125	0.079 ± 0.034	0.006 ± 0.000	4 ± 1	10 ± 4
	3	0.888 ± 0.092	0.727 ± 0.227	0.095 ± 0.040	0.022 ± 0.012	6 ± 2	31 ± 18
	4	0.921 ± 0.064	0.468 ± 0.125	0.080 ± 0.017	0.039 ± 0.020	8 ± 3	44 ± 29
	5	0.805 ± 0.137	0.541 ± 0.210	0.067 ± 0.023	0.081 ± 0.034	12 ± 4	97 ± 55
	6	0.816 ± 0.164	0.500 ± 0.148	0.076 ± 0.008	0.255 ± 0.239	16 ± 6	202 ± 180
	7	0.776 ± 0.158	0.483 ± 0.146	0.070 ± 0.009	0.333 ± 0.346	20 ± 4	216 ± 119
	8	0.641 ± 0.093	0.620 ± 0.126	0.075 ± 0.009	0.410 ± 0.238	27 ± 3	342 ± 124
	9	0.625 ± 0.205	0.642 ± 0.126	0.064 ± 0.014	1.249 ± 0.939	33 ± 7	751 ± 479
	10	0.785 ± 0.222	0.505 ± 0.112	0.075 ± 0.005	0.973 ± 1.301	30 ± 7	690 ± 580
	11	0.840 ± 0.217	0.557 ± 0.162	0.074 ± 0.005	0.746 ± 0.663	38 ± 7	812 ± 729
	12	0.790 ± 0.284	0.623 ± 0.225	0.072 ± 0.018	1.896 ± 2.837	38 ± 11	1132 ± 1419
	Weight anomaly	2	0.898 ± 0.140	0.911 ± 0.124	0.082 ± 0.040	0.005 ± 0.001	4 ± 0
3		0.750 ± 0.162	0.783 ± 0.230	0.075 ± 0.019	0.017 ± 0.009	7 ± 1	29 ± 11
4		0.841 ± 0.076	0.665 ± 0.207	0.066 ± 0.011	0.048 ± 0.052	10 ± 2	64 ± 24
5		0.840 ± 0.148	0.538 ± 0.196	0.065 ± 0.015	0.082 ± 0.063	10 ± 3	101 ± 55
6		0.719 ± 0.167	0.609 ± 0.218	0.060 ± 0.022	0.303 ± 0.345	17 ± 5	189 ± 82
7		0.713 ± 0.228	0.615 ± 0.185	0.052 ± 0.024	0.348 ± 0.298	21 ± 5	303 ± 170
8		0.639 ± 0.187	0.630 ± 0.180	0.050 ± 0.018	0.657 ± 0.428	23 ± 4	419 ± 167
9		0.714 ± 0.175	0.564 ± 0.156	0.059 ± 0.020	0.837 ± 0.576	29 ± 6	526 ± 312
10		0.582 ± 0.130	0.606 ± 0.153	0.055 ± 0.021	2.361 ± 3.487	33 ± 9	1164 ± 627
11		0.712 ± 0.268	0.635 ± 0.198	0.055 ± 0.020	1.017 ± 0.688	37 ± 9	880 ± 514
12		0.679 ± 0.234	0.628 ± 0.167	0.054 ± 0.022	1.653 ± 2.204	38 ± 10	1031 ± 640

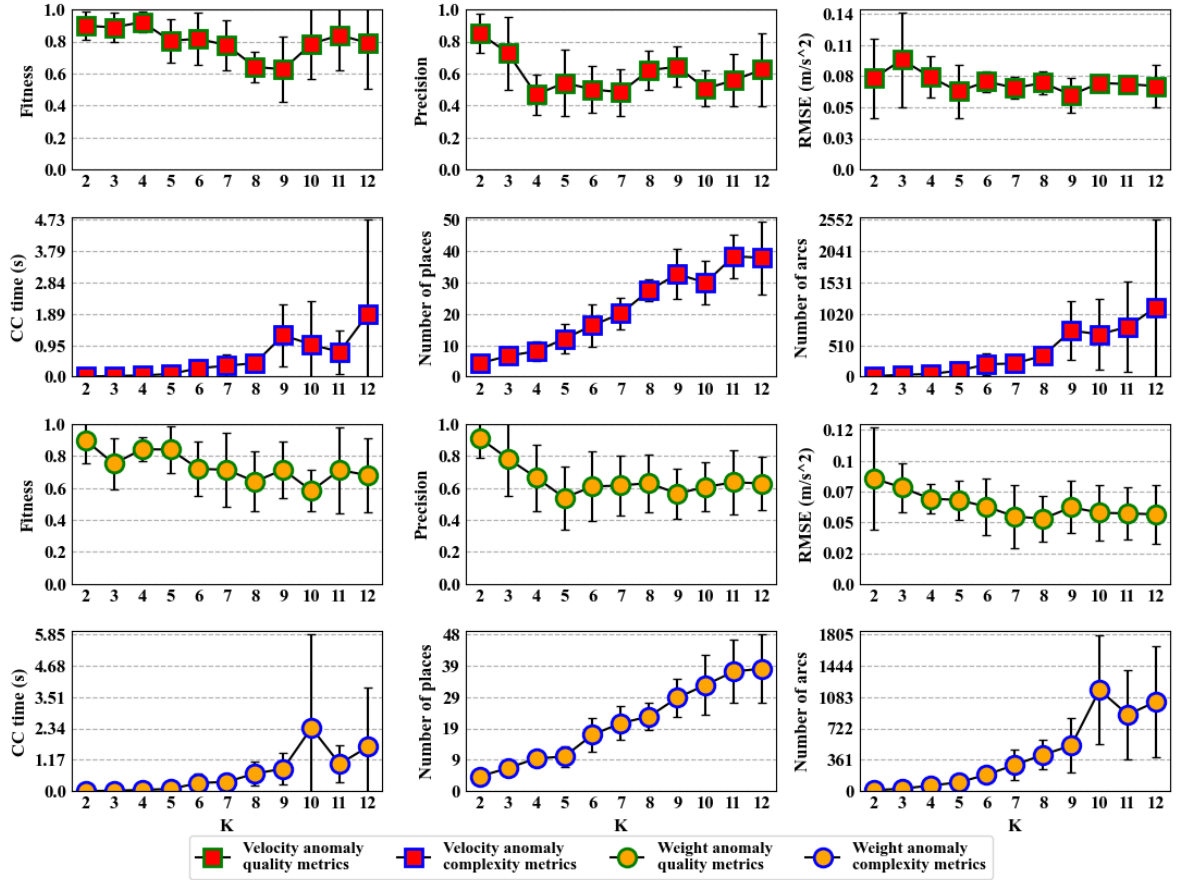


Figure 6: Quality metrics (fitness, precision, RMSE) and complexity metrics (conformance checking (CC) time, number of places, number of arcs) error bars per K value and anomaly type obtained with the ILP with 75% noise tolerance.

Table 3: Methodology results of the IMf regarding the *velocity* and *weight* anomalies showing the mean fitness, precision, RMSE, conformance checking (CC) time, number of places, and number of arcs for each K. Highlighted in bold are the Petri nets with the lowest RMSE.

		IMf (75% noise threshold)						
		K	F	P	RMSE ($\frac{m}{s}$)	CC time (s)	Places	Arcs
Velocity anomaly	2	0.901 ± 0.089	0.788 ± 0.134	0.086 ± 0.032	0.016 ± 0.025	4 ± 0	10 ± 2	
	3	0.833 ± 0.105	0.780 ± 0.139	0.089 ± 0.040	0.034 ± 0.040	7 ± 1	29 ± 11	
	4	0.744 ± 0.103	0.649 ± 0.215	0.092 ± 0.032	0.050 ± 0.048	10 ± 2	64 ± 24	
	5	0.619 ± 0.128	0.675 ± 0.153	0.080 ± 0.016	0.062 ± 0.025	10 ± 3	101 ± 55	
	6	0.668 ± 0.138	0.531 ± 0.170	0.074 ± 0.006	0.433 ± 0.483	17 ± 5	189 ± 82	
	7	0.608 ± 0.096	0.425 ± 0.156	0.076 ± 0.004	0.613 ± 0.561	21 ± 5	303 ± 170	
	8	0.542 ± 0.116	0.292 ± 0.189	0.078 ± 0.013	0.822 ± 0.865	23 ± 4	419 ± 167	
	9	0.541 ± 0.078	0.317 ± 0.158	0.067 ± 0.014	13.53 ± 25.55	29 ± 6	526 ± 312	
	10	0.579 ± 0.108	0.576 ± 0.128	0.101 ± 0.039	2.408 ± 3.233	33 ± 9	1164 ± 627	
	11	0.509 ± 0.105	0.398 ± 0.262	0.100 ± 0.039	30.198 ± 65.617	37 ± 9	880 ± 514	
	12	0.790 ± 0.284	0.324 ± 0.320	0.076 ± 0.022	22.161 ± 32.030	38 ± 10	1031 ± 640	
	Weight anomaly	2	0.919 ± 0.075	0.826 ± 0.167	0.078 ± 0.037	0.005 ± 0.002	5 ± 1	11 ± 3
3		0.794 ± 0.085	0.607 ± 0.256	0.078 ± 0.023	0.016 ± 0.008	7 ± 1	19 ± 5	
4		0.662 ± 0.177	0.657 ± 0.142	0.078 ± 0.055	0.037 ± 0.025	10 ± 2	29 ± 7	
5		0.660 ± 0.179	0.482 ± 0.313	0.088 ± 0.044	0.057 ± 0.038	14 ± 3	38 ± 10	
6		0.536 ± 0.132	0.341 ± 0.236	0.114 ± 0.058	0.232 ± 0.253	19 ± 5	53 ± 16	
7		0.578 ± 0.145	0.332 ± 0.202	0.063 ± 0.029	1.169 ± 1.873	28 ± 7	82 ± 26	
8		0.403 ± 0.214	0.265 ± 0.212	0.082 ± 0.038	0.517 ± 0.371	29 ± 6	78 ± 17	
9		0.514 ± 0.149	0.414 ± 0.274	0.068 ± 0.026	10.560 ± 25.965	36 ± 11	97 ± 35	
10		0.468 ± 0.184	0.410 ± 0.258	0.061 ± 0.019	14.164 ± 33.215	45 ± 15	126 ± 53	
11		0.508 ± 0.108	0.421 ± 0.180	0.076 ± 0.018	30.900 ± 54.842	51 ± 11	134 ± 31	
12		0.410 ± 0.199	0.383 ± 0.319	0.069 ± 0.020	16.631 ± 45.341	54 ± 17	143 ± 55	

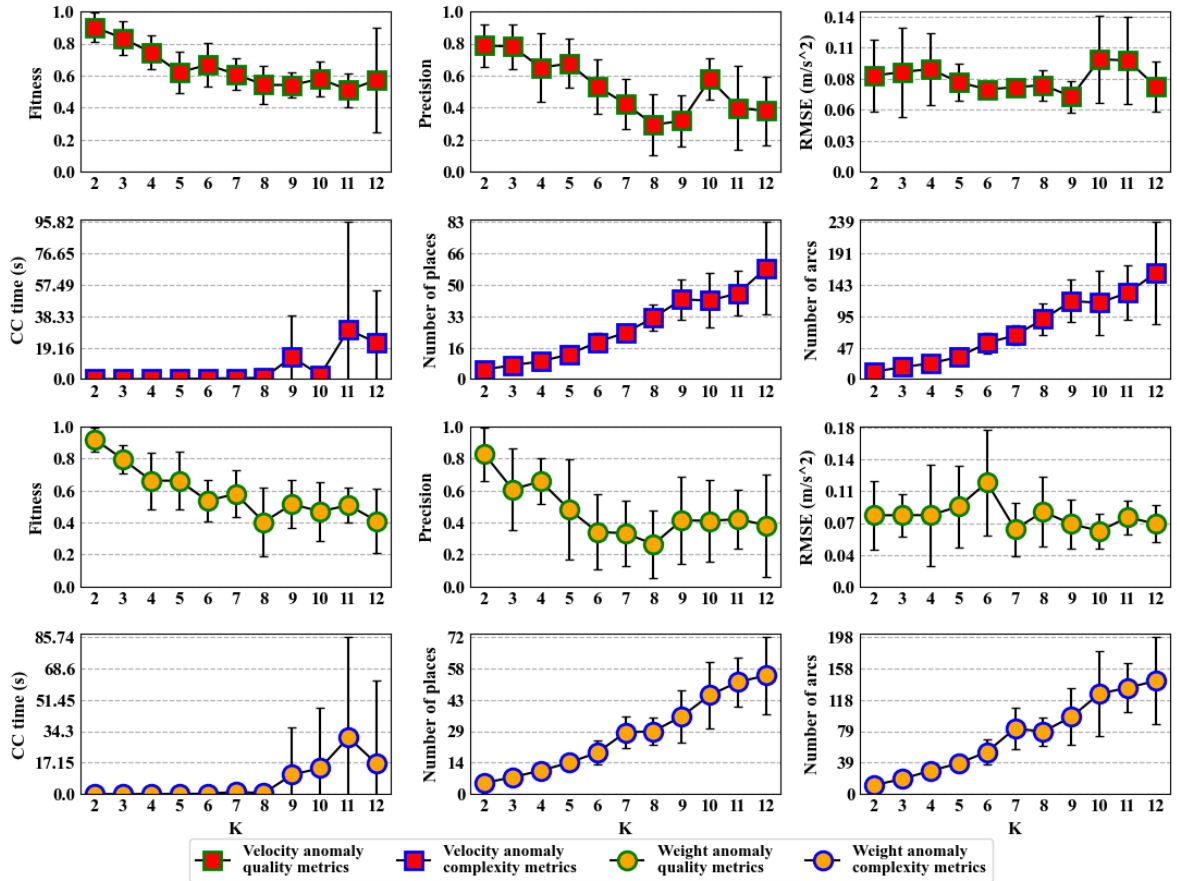


Figure 7: Quality metrics (fitness, precision, RMSE) and complexity metrics (conformance checking (CC) time, number of places, number of arcs) error bars per K value and anomaly type obtained with the IMf with 75% noise tolerance.

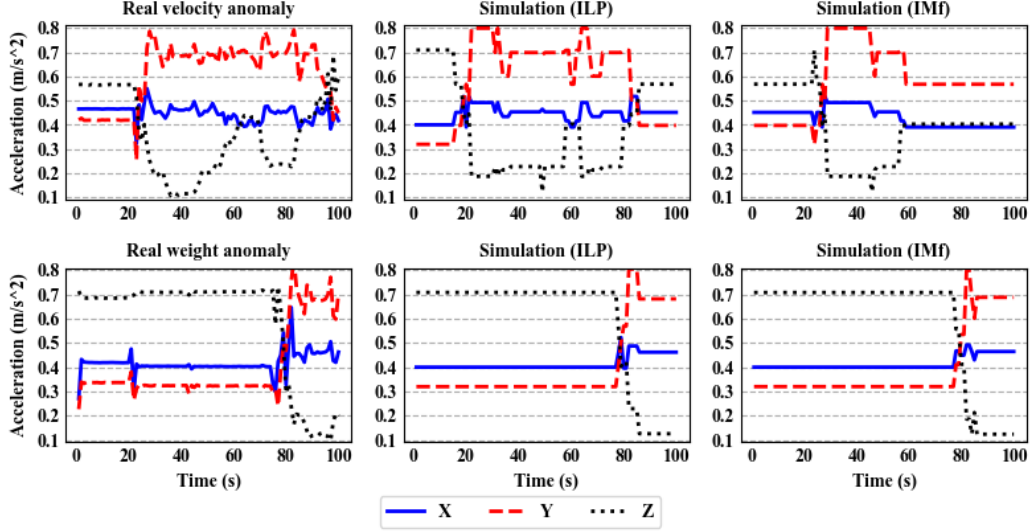


Figure 8: Comparison of the acceleration along the X, Y, and Z axes of real and simulated anomalies.

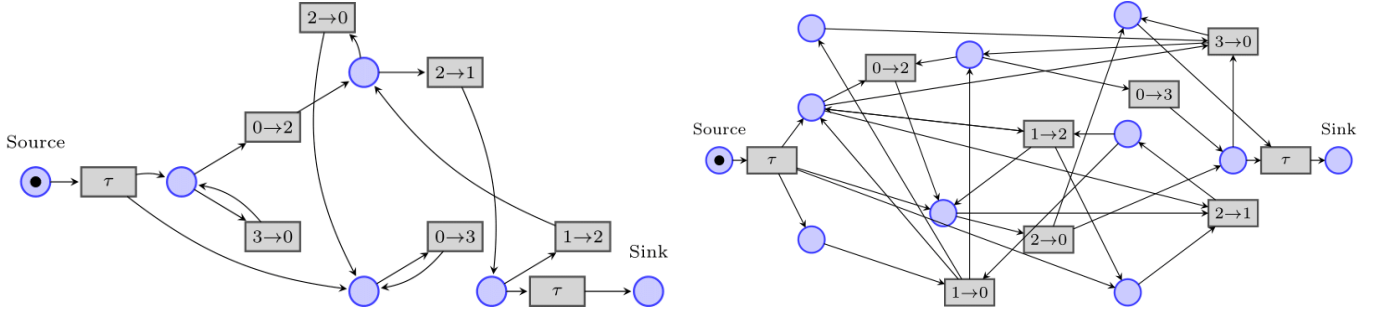


Figure 9: Velocity (left) and weight (right) Petri nets obtained by the ILP with K equal to 4.

Table 4: Fitness values and ratios for the velocity ($F_{Velocity}$) and weight (F_{Weight}) anomaly types for each K value using the ILP. Highlighted in bold are the velocity and weight Petri nets with the best RMSE. The grey rows highlight the Petri nets corresponding to those shown in Figure 9.

K	Velocity anomaly			Weight anomaly		
	$F_{Velocity}$	F_{Weight}	$F_{Velocity}/F_{Weight}$	$F_{Velocity}$	F_{Weight}	$F_{Weight}/F_{Velocity}$
2	0.912 ± 0.078	0.799 ± 0.117	1.162 ± 0.196	0.774 ± 0.210	0.898 ± 0.140	1.304 ± 0.664
3	0.787 ± 0.291	0.552 ± 0.240	1.482 ± 0.302	0.624 ± 0.287	0.750 ± 0.162	1.163 ± 0.447
4	0.810 ± 0.303	0.582 ± 0.261	1.500 ± 0.553	0.601 ± 0.303	0.841 ± 0.076	1.532 ± 1.018
5	0.718 ± 0.276	0.591 ± 0.304	1.325 ± 0.364	0.516 ± 0.235	0.840 ± 0.148	1.568 ± 0.602
6	0.825 ± 0.151	0.463 ± 0.116	1.926 ± 0.674	0.523 ± 0.125	0.719 ± 0.168	1.462 ± 0.571
7	0.808 ± 0.147	0.436 ± 0.116	1.949 ± 0.471	0.428 ± 0.148	0.713 ± 0.228	1.795 ± 0.636
8	0.682 ± 0.393	0.393 ± 0.112	1.882 ± 0.713	0.361 ± 0.090	0.639 ± 0.187	1.889 ± 0.669
9	0.692 ± 0.234	0.327 ± 0.070	2.199 ± 0.857	0.339 ± 0.090	0.714 ± 0.175	2.287 ± 0.845
10	0.742 ± 0.215	0.263 ± 0.063	3.006 ± 1.242	0.320 ± 0.102	0.582 ± 0.130	2.243 ± 1.590
11	0.810 ± 0.216	0.293 ± 0.099	3.133 ± 1.491	0.343 ± 0.074	0.711 ± 0.268	2.189 ± 0.926
12	0.793 ± 0.283	0.220 ± 0.070	4.238 ± 2.422	0.283 ± 0.088	0.679 ± 0.234	3.105 ± 3.076

the ILP and IMf, although the ILP showed overall better performance, especially in regards to the conformance checking time, which, instead, reached very high figures for the IMf. In addition, we studied the space complexity of the obtained Petri nets, which obviously increases as K becomes higher. Such a space complexity increase leads to unreadable Petri nets, impairing their interpretability. Hence, a balance between quality and complexity must be ensured to maintain the advantages of using the proposed method.

Fault identification. Next, we evaluated whether the methodology allowed distinguishing the two different anomaly types. Interestingly, although low K values lead to high fitness values when applying conformance checking between the target anomaly type and its model, high fitness values are also achieved by comparing the other anomaly type with the same model. This confirms an intuitive concept: the simpler the state space of the Petri net, the harder it is to distinguish anomalies from one another. In other words, the Petri net is underfitting

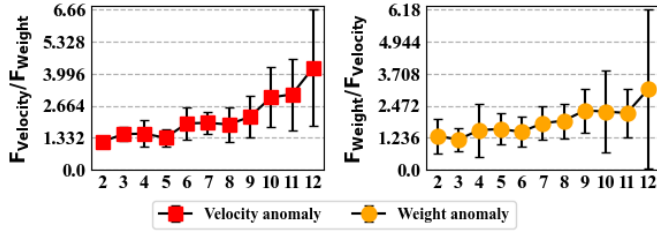


Figure 10: Fitness ratios for the velocity ($F_{Velocity}$) and weight (F_{Weight}) anomaly types for each K value using the ILP.

since it is not able to distinguish different anomaly types. On the contrary, high K values maintain high fitness values when applying conformance checking between the target anomaly type and its model, while ensuring low fitness values for the other anomaly, demonstrating the ability to identify different faults with a more complex state space.

4.6. Threats to validity

The threats to validity regard possible construct, internal and external pitfalls in the experimentation.

Construct validity. Since our focus was not on evaluating the impact of data pre-processing and anomaly detection on the experimental results, we set default configurations for these phases. These included normalizing acceleration values between -1 and 1, selecting a specific sensor for data collection, defining the number of raw sensor data samples, and grouping similar time series windows before applying subsequent methodological phases. While these choices streamlined our experiments, they may have influenced the results in ways not explicitly accounted for.

Internal validity. We observed correlations between the state space complexity of the Petri net, the chosen process discovery algorithms, and trends in process model quality and fault identification metrics, as shown in Tables 2, 3 and 4, and Figures 6, 7 and 10. However, other factors may also have influenced these metrics. For instance, variations in anomaly detection outcomes or the filtering effects of different process discovery algorithms could have played a significant role in shaping the results.

External validity. Our study focused on the RoAD case study, which involved real multivariate time series data collected from various sensors mounted on a Kuka LBR iiwa robotic arm. While this dataset provides a solid foundation for evaluation, applying our methodology to additional CPSs would further strengthen the generalizability of our findings. Future studies could validate these results across different CPS environments to assess their broader applicability.

5. Conclusions

The ever-increasing functional complexity of contemporary CPSs heightens their vulnerability to latent faults and cascading anomalies. Reliable operation, therefore, hinges on diagnosis

techniques that (i) pinpoint root causes and (ii) support *what-if* analyses through realistic simulation. Yet constructing faithful behavioral models by hand is both error-prone and knowledge-intensive. This study has demonstrated that *process mining* and, specifically, the discovery of interpretable Petri nets enriched with stochastic timing information offers a principled, data-driven alternative.

We introduced an *unsupervised* methodology that isolates anomalous sensor windows, converts them into event logs, and automatically derives stochastic Petri nets able to replicate and explain faulty dynamics. Extensive experiments on the Robotic Arm Dataset (RoAD) a widely adopted benchmark for manufacturing CPSs show that the resulting models (i) fit observed fault traces with high precision, (ii) generate realistic simulation scenarios, and (iii) enable the construction of a concise fault dictionary for on-line classification. Collectively, these findings confirm the viability of process-mining derived models as transparent, executable knowledge sources for CPS dependability analyses.

Future research will focus on three directions. First, applying the pipeline to additional industrial domains (e.g., smart grids and autonomous vehicles) will further assess its generalizability. Second, integrating the discovered fault models with predictive-maintenance platforms may unlock early-warning capabilities and optimize maintenance scheduling. Finally, coupling the simulation component with formal safety mechanisms, such as runtime monitors or digital-twin-based controllers, could provide quantitative evidence of system resilience under rare but critical fault scenarios.

Declaration of competing interest

The authors declare that they have no known competing financial interests or personal relationships that could have appeared to influence the work reported in this paper.

Acknowledgments

This study is supported by the Spoke 9 “Digital Society & Smart Cities” of ICSC - Centro Nazionale di Ricerca in High Performance-Computing, Big Data and Quantum Computing, funded by the European Union - NextGenerationEU (PNRR-HPC, CUP: E63C22000980007), and by the European Union’s Horizon Europe research and innovation programme under the Marie Skłodowska-Curie grant agreement No. 101109243. This manuscript reflects only the Authors’ views and opinions, neither the European Union nor the European Commission can be considered responsible for them.

Data availability

The code and dataset for this paper are available in the following GitHub repository: https://github.com/francescovitale/pm_based_modeling_simulation.

References

- Adriansyah, A., Munoz-Gama, J., Carmona, J., Van Dongen, B. F., & van der Aalst, W. M. P. (2015). Measuring precision of modeled behavior. *Information systems and e-Business Management*, 13, 37–67. <https://doi.org/10.1007/s10257-014-0234-7>
- Belay, M. A., Rasheed, A., & Rossi, P. S. (2024). MTAD: Multiobjective Transformer Network for Unsupervised Multisensor Anomaly Detection. *IEEE Sensors Journal*, 24(12), 20254–20265. <https://doi.org/10.1109/JSEN.2024.3396690>
- Beyel, H. H., Makke, O., Pourbafrani, M., Gusikhin, O., & van der Aalst, W. M. P. (2024). Analyzing Data Streams from Cyber-Physical-Systems: A Case Study. *SN Computer Science*, 5, 1–17. <https://doi.org/10.1007/s42979-024-03008-8>
- Bonafin, A. C., Cabral, F. G., & Moreira, M. V. (2022). An effective approach for fault diagnosis of Discrete-Event Systems modeled as safe labeled Petri nets. *Control Engineering Practice*, 123, 105168. <https://doi.org/10.1016/j.conengprac.2022.105168>
- Bourdeau, M., qiang Zhai, X., Nefzaoui, E., Guo, X., & Chatellier, P. (2019). Modeling and forecasting building energy consumption: A review of data-driven techniques. *Sustainable Cities and Society*, 48, 101533. <https://doi.org/10.1016/j.scs.2019.101533>
- Cabasino, M., Giua, A., Poggi, M., & Seatzu, C. (2011). Discrete event diagnosis using labeled Petri nets. An application to manufacturing systems. *Control Engineering Practice*, 19(90), 989–1001. <https://doi.org/10.1016/j.conengprac.2010.12.010>
- Cai, B., Huang, L., & Xie, M. (2017). Bayesian Networks in Fault Diagnosis. *IEEE Transactions on Industrial Informatics*, 13, 2227–2240. <https://doi.org/10.1109/TII.2017.2695583>
- Carmona, J., van Dongen, B., Solti, A., & Weidlich, M. (2018). *Conformance Checking: Relating Processes and Models*. Springer Publishing Company, Incorporated. <https://doi.org/10.1007/978-3-319-99414-7>
- Chandola, V., Banerjee, A., & Kumar, V. (2012). Anomaly Detection for Discrete Sequences: A Survey. *IEEE Transactions on Knowledge and Data Engineering*, 24(5), 823–839. <https://doi.org/10.1109/TKDE.2010.235>
- Chatterjee, A., & Ahmed, B. S. (2022). IoT anomaly detection methods and applications: A survey. *Internet of Things*, 19, 100568. <https://doi.org/10.1016/j.iot.2022.100568>
- Cook, A. A., Misirli, G., & Fan, Z. (2020). Anomaly Detection for IoT Time-Series Data: A Survey. *IEEE Internet of Things Journal*, 7, 6481–6494. <https://doi.org/10.1109/JIOT.2019.2958185>
- da Silveira, A. C., Álvaro Sobrinho, Dias da Silva, L., Santos, D. F., Nauman, M., & Perkusich, A. (2025). Harnessing coloured Petri nets to enhance machine learning: A simulation-based method for healthcare and beyond. *Simulation Modelling Practice and Theory*, 140, 103080. <https://doi.org/10.1016/j.simpat.2025.103080>
- De Benedictis, A., Flammini, F., Mazzocca, N., Somma, A., & Vitale, F. (2023). Digital Twins for Anomaly Detection in the Industrial Internet of Things: Conceptual Architecture and Proof-of-Concept. *IEEE Transactions on Industrial Informatics*, 19(12), 11553–11563. <https://doi.org/10.1109/TII.2023.3246983>
- Feng, H., Gomes, C., Gil, S., Mikkelsen, P. H., Tola, D., Larsen, P. G., & Sandberg, M. (2022). Integration Of The Mape-K Loop In Digital Twins. In *2022 Annual Modeling and Simulation Conference (ANNSIM)* (pp. 102–113). <https://doi.org/10.23919/ANNSIM55834.2022.9859489>
- Friederich, J., & Lazarova-Molnar, S. (2022). Data-Driven Reliability Modeling of Smart Manufacturing Systems Using Process Mining. In *2022 Winter Simulation Conference (WSC)* (pp. 2534–2545). <https://doi.org/10.1109/WSC57314.2022.10015301>
- Golendukhina, V., Wiesmayr, B., & Felderer, M. (2024). A Review of Publicly Available Datasets from Manufacturing Systems. In *2024 IEEE 29th International Conference on Emerging Technologies and Factory Automation (ETFA)* (pp. 1–8). <https://doi.org/10.1109/ETFA61755.2024.10710865>
- Gueuziec, B., Gallois, J., & Boulanger, F. (2023). Qualitative Tendencies for Hybrid System Simulation. In *2023 ACM/IEEE International Conference on Model Driven Engineering Languages and Systems Companion (MODELS-C)* (pp. 500–509). <https://doi.org/10.1109/MODELS-C59198.2023.00087>
- Hanga, K. M., Kovalchuk, Y., & Gaber, M. M. (2020). A Graph-Based Approach to Interpreting Recurrent Neural Networks in Process Mining. *IEEE Access*, 8, 172923–172938. <https://doi.org/10.1109/ACCESS.2020.3025999>
- Hemmer, A., Abderrahim, M., Badonnel, R., François, J., & Chriment, I. (2021). Comparative Assessment of Process Mining for Supporting IoT Predictive Security. *IEEE Transactions on Network and Service Management*, 18(1), 1092–1103. <https://doi.org/10.1109/TNSM.2020.3038172>
- Hou, W., Ye, J., & Wang, J. (2021). Fault identification of DES using Petri net. In *2021 IEEE International Conference on Networking, Sensing and Control (ICNSC)* (pp. 1–6). <https://doi.org/10.1109/ICNSC52481.2021.9702163>
- Hu, S., Li, Z., & Wisniewski, R. (2024). Optimal Sensor Selection for Diagnosability Enforcement in Labeled Petri Nets. *IEEE Transactions on Systems, Man, and Cybernetics: Systems*, 54, 2965–2977. <https://doi.org/10.1109/TSMC.2024.3351740>
- Khan, U., Cheng, D., Setti, F., Fummi, F., Cristani, M., & Capogrosso, L. (2025). A Comprehensive Survey on Deep Learning-based Predictive Maintenance. *ACM Transactions on Embedded Computing Systems*. <https://doi.org/10.1145/3732287>
- Lassoued, S., & Schwung, A. (2024). Introducing PetriRL: An innovative framework for JSSP resolution integrating Petri nets and event-based reinforcement learning. *Jour-*

- nal of Manufacturing Systems*, 74, 690-702. <https://doi.org/10.1016/j.jmsy.2024.04.028>
- Leemans, S. J. J., Fahland, D., & van der Aalst, W. M. P. (2013). Discovering Block-Structured Process Models from Event Logs - A Constructive Approach. In *Application and Theory of Petri Nets and Concurrency* (pp. 311–329). https://doi.org/10.1007/978-3-642-38697-8_17
- Leemans, S. J. J., Fahland, D., & van der Aalst, W. M. P. (2014). Discovering Block-Structured Process Models from Event Logs Containing Infrequent Behaviour. In *Business Process Management Workshops* (pp. 66–78). https://doi.org/10.1007/978-3-319-06257-0_6
- Li, C., Li, S., Wang, H., Gu, F., & Ball, A. D. (2023). Attention-based deep meta-transfer learning for few-shot fine-grained fault diagnosis. *Knowledge-Based Systems*, 264, 110345. <https://doi.org/10.1016/j.knosys.2023.110345>
- Liu, H., Wang, Y., Fan, W., Liu, X., Li, Y., Jain, S., ... Tang, J. (2022). Trustworthy AI: A Computational Perspective. *ACM Transactions on Intelligent Systems and Technology*, 14(1), 1–59. <https://doi.org/10.1145/3546872>
- Liu, J., Mvungi, E. S. B., Zhang, X., & Dias, A. (2024). Fault Diagnosis in Partially Observable Petri Nets with Quantum Bayesian Learning. *Applied Sciences*, 14, 1–52. <https://doi.org/10.3390/app14010052>
- Liu, S., Hu, X., & Wang, J. (2013). Hierarchical Modeling Fault-Error-Failure Dependencies for Cyber-Physical Systems. In *Proceedings of The Eighth International Conference on Bio-Inspired Computing: Theories and Applications (BIC-TA), 2013* (pp. 641–649). https://doi.org/10.1007/978-3-642-37502-6_77
- Mansour, M., Wahab, M. A., & Soliman, W. M. (2013). Petri nets for fault diagnosis of large power generation station. *Ain Shams Engineering Journal*, 4(4), 831-842. <https://doi.org/10.1016/j.asej.2013.04.006>
- Mascolini, A., Gaiardelli, S., Ponzio, F., Dall’Ora, N., Macii, E., Vinco, S., ... Fummi, F. (2023). Robotic Arm Dataset (RoAD): A Dataset to Support the Design and Test of Machine Learning-Driven Anomaly Detection in a Production Line. In *IECON 2023- 49th Annual Conference of the IEEE Industrial Electronics Society* (pp. 1–7). <https://doi.org/10.1109/IECON51785.2023.10311726>
- Ming, Z., Tang, B., Deng, L., Yang, Q., & Li, Q. (2025). Digital twin-assisted fault diagnosis framework for rolling bearings under imbalanced data. *Applied Soft Computing*, 168, 112528. <https://doi.org/10.1016/j.asoc.2024.112528>
- Mozafari Mehr, A. S., M. de Carvalho, R., & van Dongen, B. (2023). Explainable conformance checking: Understanding patterns of anomalous behavior. *Engineering Applications of Artificial Intelligence*, 126, 106827. <https://doi.org/10.1016/j.engappai.2023.106827>
- Nadim, K., Ragab, A., & Ouali, M.-S. (2022, May). Data-driven dynamic causality analysis of industrial systems using interpretable machine learning and process mining. *Journal of Intelligent Manufacturing*, 34(1), 57–83. <https://doi.org/10.1007/s10845-021-01903-y>
- Nazemzadeh, P., Dideban, A., & Zareiee, M. (2013). Fault Modeling in Discrete Event Systems Using Petri Nets. *ACM Transactions on Embedded Computing Systems*, 12. <https://doi.org/10.1145/2406336.2406348>
- Neshastegaran, A., Norouzifar, A., & Izadi, I. (2022). A Framework for Plant Topology Extraction Using Process Mining and Alarm Data. In *2022 30th International Conference on Electrical Engineering (ICEE)* (pp. 485–491). <https://doi.org/10.1109/ICEE55646.2022.9827266>
- Oks, S. J., Jalowski, M., Lechner, M., Mirschberger, S., Merklein, M., Vogel-Heuser, B., & Möslin, K. M. (2024). Cyber-physical systems in the context of industry 4.0: A review, categorization and outlook. *Information Systems Frontiers*, 26, 1731—1772. <https://doi.org/10.1007/s10796-022-10252-x>
- Paparrizos, J., & Gravano, L. (2016). k-Shape: Efficient and Accurate Clustering of Time Series. *ACM SIGMOD Record*, 45, 69—76. <https://doi.org/10.1145/2949741.2949758>
- Qin, H., Zhan, X., & Zheng, Y. (2023). CSCAD: Correlation Structure-Based Collective Anomaly Detection in Complex System. *IEEE Transactions on Knowledge and Data Engineering*, 35(5), 4634–4645. <https://doi.org/10.1109/TKDE.2022.3154166>
- Rogge-Solti, A., van der Aalst, W. M. P., & Weske, M. (2014). Discovering Stochastic Petri Nets with Arbitrary Delay Distributions from Event Logs. In *Business process management workshops* (pp. 15–27). https://doi.org/10.1007/978-3-319-06257-0_2
- Shi, Y., Zhang, N., Song, X., Li, H., & Zhu, Q. (2024). Novel approach for industrial process anomaly detection based on process mining. *Journal of Process Control*, 136, 103165. <https://doi.org/10.1016/j.jprocont.2024.103165>
- Su, Z., Yu, T., Polyvyanyy, A., Tan, Y., Lipovetzky, N., Sardiña, S., ... Oetomo, D. (2025). Process mining over sensor data: Goal recognition for powered transhumeral prostheses. *Information Systems*, 132, 102540. <https://doi.org/10.1016/j.is.2025.102540>
- Tampouratzis, N., Mousoulitios, P., & Papaefstathiou, I. (2023). A Novel Integrated Simulation Framework for Cyber-Physical Systems Modelling. *IEEE Transactions on Parallel and Distributed Systems*, 34(10), 2684–2698. <https://doi.org/10.1109/TPDS.2023.3300081>
- van der Aalst, W. M. P., & Carmona, J. (2022). *Process Mining Handbook*. Cham, Switzerland: Springer. <https://doi.org/10.1007/978-3-031-08848-3>
- van Eck, M. L., Sidorova, N., & van der Aalst, W. M. P. (2016). Enabling process mining on sensor data from smart products. In *2016 IEEE Tenth International Conference on Research Challenges in Information Science (RCIS)* (pp. 1–12). <https://doi.org/10.1109/RCIS.2016.7549355>
- van Zelst, S. J., van Dongen, B. F., van der Aalst, W. M., & Verbeek, H. M. (2018). Discovering workflow nets using integer linear programming. *Computing*, 100, 529–556. <https://doi.org/10.1007/s00607-017-0582-5>
- Vitale, F., De Vita, F., Mazzocca, N., & Bruneo, D. (2023). A Process Mining-based unsupervised Anomaly Detection

- technique for the Industrial Internet of Things. *Internet of Things*, 24, 100993. <https://doi.org/10.1016/j.iot.2023.100993>
- Vitale, F., Guarino, S., Flammini, F., Faramondi, L., Mazzocca, N., & Setola, R. (2025). Process Mining for Digital Twin Development of Industrial Cyber-Physical Systems. *IEEE Transactions on Industrial Informatics*, 21(1), 866–875. <https://doi.org/10.1109/TII.2024.3465600>
- Wang, X., Yang, L., Li, D., Ma, L., He, Y., Xiao, J., . . . Yang, Y. (2022). MADDC: Multi-Scale Anomaly Detection, Diagnosis and Correction for Discrete Event Logs. In *Proceedings of the 38th annual computer security applications conference* (p. 769—784). <https://doi.org/10.1145/3564625.3567972>
- Wittbold, F., Bernemann, R., Heckel, R., Heindel, T., & König, B. (2023). Stochastic decision petri nets. In *Application and theory of petri nets and concurrency* (pp. 264–285).
- Yu, W., & Zhao, C. (2020). Broad Convolutional Neural Network Based Industrial Process Fault Diagnosis With Incremental Learning Capability. *IEEE Transactions on Industrial Electronics*, 67(6), 5081-5091. <https://doi.org/10.1109/TIE.2019.2931255>
- Zamanzadeh Darban, Z., Webb, G. I., Pan, S., Aggarwal, C., & Salehi, M. (2024). Deep Learning for Time Series Anomaly Detection: A Survey. *ACM Computing Surveys*, 57(1), 1–42. <https://doi.org/10.1145/3691338>
- Zhu, G., Li, Z., Wu, N., & Al-Ahmari, A. (2019). Fault Identification of Discrete Event Systems Modeled by Petri Nets With Unobservable Transitions. *IEEE Transactions on Systems, Man, and Cybernetics: Systems*, 49(2), 333–345. <https://doi.org/10.1109/TSMC.2017.2762823>